



# Kaon Production Target for Hall D at Jefferson Laboratory (Technical Note)

Igor Strakovsky,<sup>1,\*</sup> Moskov Amaryan,<sup>2</sup> Mikhail Bashkanov,<sup>3</sup> Vitaly Baturin,<sup>4</sup>  
William J. Briscoe,<sup>1</sup> Eugene Chudakov,<sup>5</sup> Pavel Degtyarenko,<sup>5</sup> Sean Dobbs,<sup>6</sup> Hovanes Egiyan,<sup>5</sup>  
Alexander Laptev,<sup>7</sup> Ilya Larin,<sup>8</sup> Alexander Somov,<sup>5</sup> and Timothy Whitlatch<sup>5</sup>

<sup>1</sup>*The George Washington University, Washington, DC 20052, USA*

<sup>2</sup>*Old Dominion University, Norfolk, VA 23529, USA*

<sup>3</sup>*University of York, Heslington, York YO10 5DD, UK*

<sup>4</sup>*Old Dominion University, Norfolk, VA 20529, USA*

<sup>5</sup>*Thomas Jefferson National Accelerator Facility, Newport News, VA 23606, USA*

<sup>6</sup>*Florida State University, Tallahassee, FL 32306, USA*

<sup>7</sup>*Los Alamos National Laboratory, Los Alamos, NM 87545, USA*

<sup>8</sup>*University of Massachusetts, Amherst, MA 01003, USA*

(Dated: July 1, 2023)

The Kaon Production Target (KPT) is an important component of the proposed K-Long Facility (KLF) for strange hadron spectroscopy in Hall D at JLab [1]. In this note we present a conceptual design for the Be-target assembly for the planned K-Long beam line, which will be used along with the GlueX spectrometer in its standard configuration for the proposed experiment. The high intensity 12 GeV CEBAF electron beam with 5  $\mu\text{A}$  current enables creation of intensive bremsstrahlung photon beam to produce the flux of  $K_L$  beam on the order of  $\sim 10^4$   $K_L/\text{sec}$  on the GlueX target exceeding the  $K_L$  flux previously obtained at SLAC by three orders of magnitude. The most important requirement for the KPT is to make sure that the neutron and the photon flux accompanying secondary  $K_L$  beam is well under control from radiation point of view. The Monte Carlo simulations for the proposed conceptual design of KPT show that the resulting neutron and gamma flux lead to a prompt radiation dose rate for the KLF experiment that is below the JLab Radiation Control Department radiation dose rate limits in the experimental hall and at the site boundary and will have no impact on the performance of the GlueX spectrometer.

## CONTENTS

	40	VI. Activation Dose	7
I. KLF Physics Case	2	VII. Simulation of Power Deposition in KPT	12
	41	A. Beam Line Model in FLUKA	12
II. The KLF Beamline	2	B. Energy Deposition in the Kaon Production Target	12
	43		
	44		
III. Proposed Concept for the Beryllium Target	3	VIII. Heating	12
A. Target and Plug Materials and Dimensions	4	A. Beryllium Target Cooling	13
B. Location of the Be-target Assembly	5		
C. The Kaon and Neutron Flux	5	IX. Summary	13
D. Neutron Flux on the Upstream Face of the GlueX Spectrometer	5		
	47		
	6	X. Acknowledgments	14
IV. Radiation Safety Requirements	7	References	15
	49		
V. Prompt Dose	7	A. KPT Shield Layers and Weight	17
	50		

\* Corresponding author; igor@gwu.edu

## I. KLF PHYSICS CASE

The GlueX spectrometer in Hall D at Jefferson Lab, shown in Figure 1, is a powerful tool employed by the GlueX Collaboration to investigate a wide range of topics in meson and baryon spectroscopy and structure, particularly the search for mesons with excited gluonic content, using the recently upgraded 12 GeV electron beam of CEBAF accelerator. The spectrometer is carefully designed to measure charged and neutral final state particles with almost  $4\pi$  acceptance.

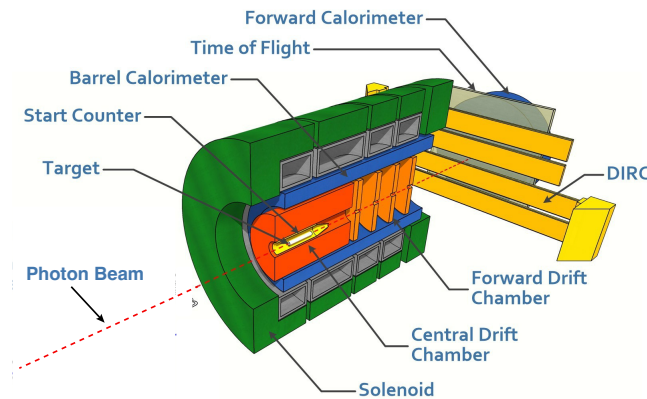


FIG. 1. The GlueX spectrometer.

The proposed secondary  $K_L$  beam at Jefferson Laboratory [1] will revolutionize our understanding of bound systems containing strange quarks by providing the long-sought, high quality experimental data required to reach deeper understanding of the role of strange quarks in hadrons. It is expected that this facility will enable significant new progress in the strange hadron spectroscopy, both in the experimental, as well as theoretical understanding of these states. It will also have a high impact on the experimental program of strange hadron spectroscopy using electromagnetic probes bringing them into a new frontier. The facility and its associated physics program would allow the hadron spectroscopy communities around the world to make an exciting new scientific advances. The existing infrastructure at Jefferson Lab is well suited to provide a new, world class kaon beam facility to enable groundbreaking progress in our field in the next decade. We are confident that obtained new experimental data will significantly enrich the physics program of the hadron spectroscopy in general and the scientific community at Jefferson Lab will continue its world leading standing in this field.

The study of the strange hadrons provides a natural motivation for the future measurements at Jefferson Lab well in accord with the long range plan summarized in **Reaching for the Horizon: Long Range Plan for Nuclear Science** [3]: *For many years, there were both theoretical and experimental reasons to believe that the strange sea-quarks might play a significant role in the nucleon's structure; a better understanding of the role of*

*strange quarks became an important priority.*

We propose to create a secondary beam of neutral kaons in Hall D at Jefferson Lab to be used with the GlueX experimental setup for the strange hadron spectroscopy [1]. The superior CEBAF electron beam will enable a flux of neutral long-lived kaons on the order of  $\sim 10^4$   $K_L$ /sec, which exceeds the kaon flux previously attained at SLAC [8] by three orders of magnitude. The use of the deuterium target in addition to the standard liquid hydrogen target will provide the first ever measurements of the neutral kaons interacting with neutrons. The ability of the GlueX spectrometer to measure reaction fragments over the wide ranges of a polar  $\theta$  and azimuthal  $\phi$  angles with a good coverage for both a charged and a neutral particles (see, for instance, Refs. [9–11]), together with the  $K_L$  momentum information from the  $K_L$  time-of-flight, provides an ideal environment for these measurements.

Our KLF proposal *Strange hadron spectroscopy with secondary  $K_L$  beam in Hall D C12-19-001* received a full approval from the PAC48 [4] to run in Hall D for 200 PAC days.

As a part of the KLF project, three new critical elements will be added to the Hall D beamline: the Compact Photon Source (CPS) [5], the Kaon Production Target (KPT) [6], and the Kaon Flux Monitor (KFM) [7].

In this work, we describe a conceptual design for the KPT that satisfies the requirements for the KLF program, and show through simulations that the expected radiation and heat deposition are within acceptable limits.

## II. THE KLF BEAMLIN

A schematic view of the proposed Hall D beam line for the KLF project showing the production chain  $e \rightarrow \gamma \rightarrow K_L$  is given in Fig. 2.

At the first stage, 12 GeV electrons with a  $5 \mu\text{A}$  current scatter off of a copper radiator ( $10\% X_0$ ) contained inside the CPS [5] generating an intense beam of untagged bremsstrahlung photons, which then travels  $\approx 65\text{m}$  towards the KPT. The energy spectrum of this photon beam that reaches the upstream end of the KPT Beryllium target is shown in Fig. 3, and has a total power of approximately 5.7 kW. The photon beam has an intensity at the KPT of  $4.7 \times 10^{12}$   $\gamma$ /sec for  $E_\gamma > 1.5$  GeV, which corresponds to the production threshold of the  $\phi$ -meson, which is the main source of the  $K_L$  beam. The remaining power of the 12 GeV, 60 kW electron beam is deposited within the CPS assembly which also acts as an electron beam dump.

The CPS will be located downstream of the Hall-D tagger magnet. The existing Hall D tagger magnet and detectors will not be used.

At the second stage, the bremsstrahlung photons hit the Be target located at the upstream end of the collimator alcove of the main experimental hall (see Fig. 5)

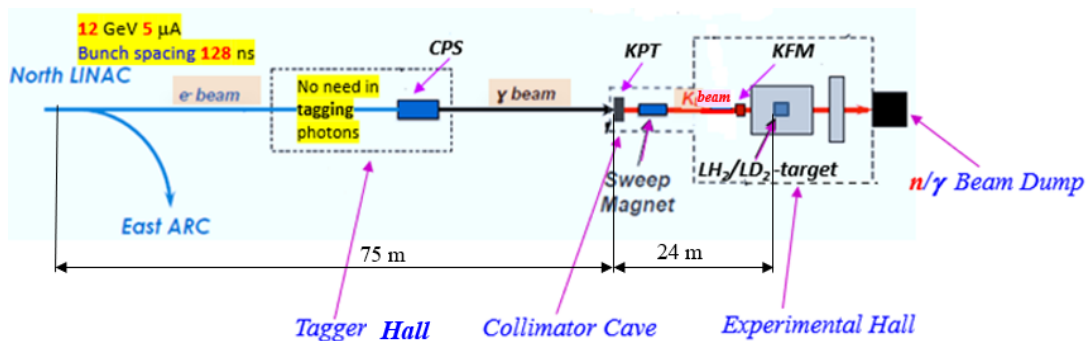


FIG. 2. Schematic view of the KLF beam line in Hall D with the production chain  $e \rightarrow \gamma \rightarrow K_L$ . The main components are the CPS, KPT, sweep magnet, and KFM (see text for details). The beam goes from the left to the right.

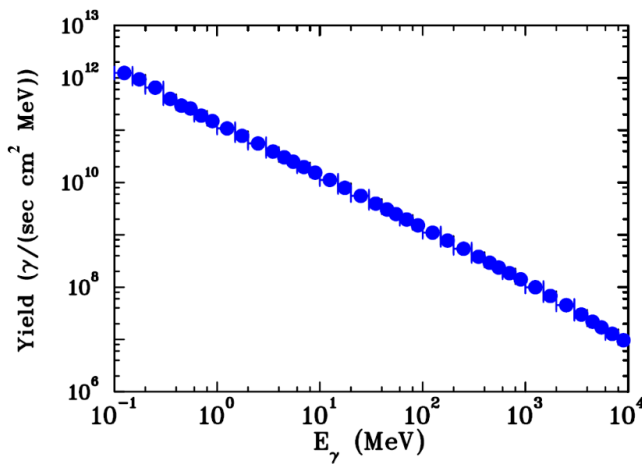


FIG. 3. The energy spectrum of the bremsstrahlung photons on the face of the Be-target. Calculations were performed using the MCNP radiation transport code [12].

and produce a beam containing neutral kaons with flux  $\sim 10^4$   $K_L$ /sec, neutrons with flux  $\sim 6.6 \times 10^5$  n/sec, a smaller flux of photons, and charged particles. The charged particles are then removed from the beam with a sweep magnet, leaving a beam that is dominantly composed of neutral kaons and neutrons.

### III. PROPOSED CONCEPT FOR THE BERYLLIUM TARGET

The KPT is built around a Beryllium target with 40 cm length and 6 cm diameter, and will be located in the collimator alcove in Hall D. This concept follows the successful use of beryllium targets for  $K_L$  production at SLAC [13] and NINA [14]. A schematic view of the Be target assembly is given in Fig. 4. In this section, we describe the design of this target assembly and the expected secondary beam characteristics.

The collimator alcove has enough room to hold the additional shielding and beam line components required

to prepare the  $K_L$  beam before it reaches the main part of the experimental hall. Since it is planned to be able to switch between the photon and  $K_L$  beam line configurations, we note that the collimator alcove is wide enough, at 4.52 m in width, for the Be target assembly to be moved to the side (Fig. 5) and remain far enough from the beam line to allow for the reinstillation of photon beam line components when switch to regular photon beam mode. Sufficient water cooling is also already available in this alcove to dissipate the approximately 5.3 kW of power delivered by the photon beam to the KPT assembly.

We have performed comprehensive simulations of the neutron, photon, and muon backgrounds to optimize the KPT design and to evaluate the resulting radiation levels and their possible influence on the performance of the GlueX detector. The most important and damaging background comes from neutrons. To estimate the neutron and gamma flux in the beam and the neutron prompt radiation dose rate in the experimental hall from scattered neutrons and gammas, we used the MCNP6 N-Particle (MCNP) radiation transport code [12].

For the MCNP calculations (in terms of flux [part/s/cm<sup>2</sup>/MeV] or biological dose rate [mrem/h]), many tallies, *i.e.*, spots where we calculated the flux or dose rate, were placed along the beam and in the experimental hall and the alcove for the neutron and gamma fluence estimation. Fluence-to-Effective Dose conversion factors from ICRP 116 [15] were implemented to convert the neutron and gamma fluences into effective dose rates. We used the material composition data for the radiation transport modeling from Ref. [16].

The MCNP simulations are based on the advanced nuclear cross section libraries created and maintained by several DOE National Laboratories. The physical models implemented in the MCNP6 code take into account bremsstrahlung photon production, photo nuclear reactions, neutrons and photons multiple scattering processes. The experimental hall, collimator alcove, and the photon beam produced in CPS were modeled using the specifications from the layout presented in Figure 5, shown as a 3D graphic model of the experimental setup.

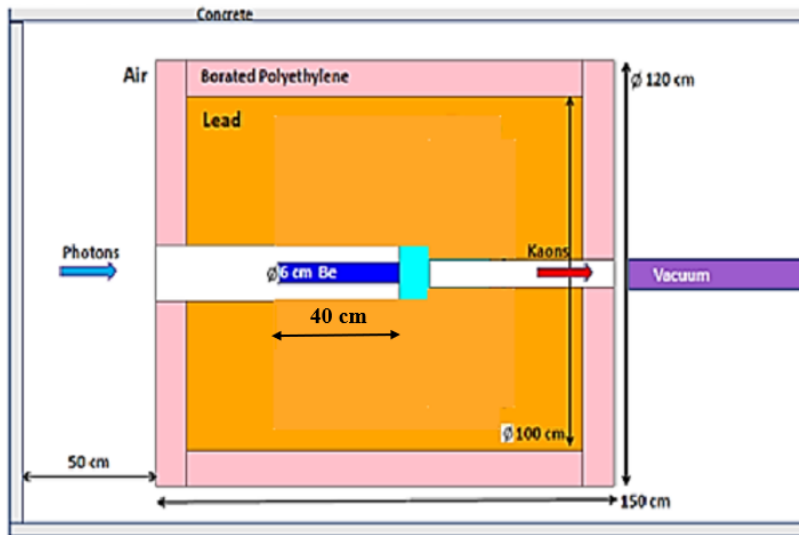


FIG. 4. fff06 Schematic view of the KPT assembly. Concrete, borated polyethylene, lead, tungsten, beryllium, vacuum beam pipe, and air shown by grey, pink, brown, light blue, blue, violet, and white colors, respectively. The beam goes from the left to the right.

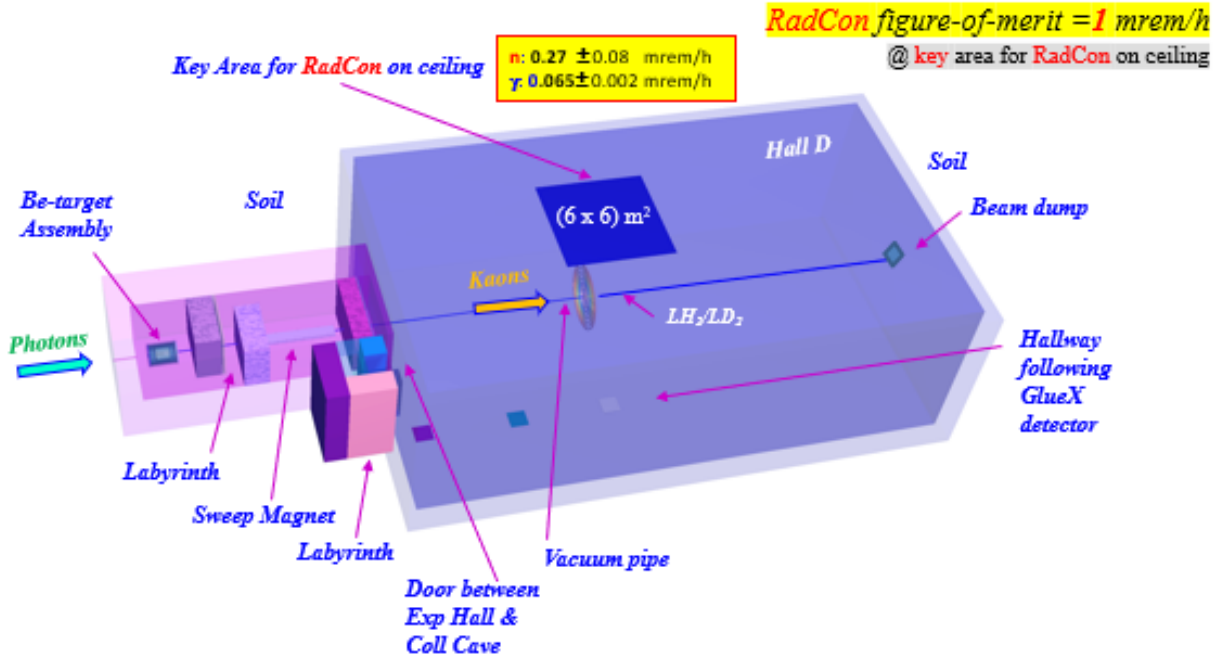


FIG. 5. fff04 Schematic view of Hall D setting for the MCNP radiation transport code [12] calculations. The model is presented as semi-transparent for demonstration purposes. The beam goes from the left to the right.

206 Additional radiation studies and calculations of power  
207 deposition were performed with the FLUKA (version  
208 FLUKA2021.2.9) software package [17].

#### A. Target and Plug Materials and Dimensions

210 The  $K_L$  beam will be produced through interactions of  
211 the photon beam with a beryllium target of 40 cm length  
212 and 6 cm diameter. The target is made of beryllium be-  
213 cause the lighter elements have a higher photoproduction  
214 yield with a lower absorption of  $K_L$ 's and a large radia-  
215 tion length, as pointed out in previous SLAC studies [21].



The length of the target was optimized by MC simulations of the  $K_L$  yield versus Be target length in a different ranges of  $K_L$  momenta shown in Fig. 6.

Other target materials that would be easier to handle than beryllium were considered, such as carbon. A mon target material could be a carbon, which is easier to handle than beryllium, however the simulations performed show that a beryllium target performs significantly better than a similar target made of carbon. However, Pythia [18] simulations showed that the kaon yield from beryllium is a factor 1.51 larger than that from carbon at the same radiation length. From MCNP simulations, we found that the absorption of neutrons in a beryllium target is about  $\sim 1.45$  larger than in a similar carbon target. From both of these considerations, beryllium is the preferred target material.

A tungsten beam plug of 10 cm thickness ( $\sim 30$  r.l.) and 16 cm diameter is attached to the downstream end of the beryllium target (as illustrated in Fig. 4) to clean up the beam and absorb induced radiation. In earlier studies at SLAC [21], it was shown that tungsten is an optimal material for the plug and that the tungsten has a lower absorption factor for kaons as compared to copper. We confirmed this effect through Pythia simulations, where we found the ratio of  $K_L$ 's surviving after a tungsten beam plug to one made of copper to be 1.16 (1.36) for kaon momentum of 1 GeV/c (0.5 GeV/c). Using MCNP simulations, we also found that the tungsten plug more effectively reduces the flux of secondary neutrons and photons compared to lead or copper of the same length. The positive effect of tungsten material compared to lead (copper) was found to be 2.25 (9.29) times lower flux of neutrons and 8.11 (66.8) for photons.

The yield of kaons from the tungsten plug was estimated to be negligible compared to the rate of kaons produced in the beryllium target. From these considerations, tungsten is the preferred beam plug material.

The dimensions of the tungsten plug were also optimized. It was found that increasing the plug diameter will increase the neutron background. For example, increasing the diameter to 24 cm from 16 cm yields an increase of neutron production by a factor of 2.8. This effect is due to re-scattered neutrons in the plug. However, there is no significant effect for photons.

It was also found that increasing the plug length will decrease the neutron and photon backgrounds. For example, increasing the plug length to 15 cm from 10 cm results factor of 0.6 for neutron production, and even a larger factor for photon production. However, increasing the plug length also reduces the number of  $K_L$ 's which exit the KPT. Therefore, we take the final length to be 10 cm.

## B. Location of the Be-target Assembly

To reduce the effect of the neutron and photon background coming from the beryllium target and tungsten

plug into the experimental hall, we place the KPT upstream of the GlueX spectrometer in the collimator alcove (see Fig. 5). Additional shielding inside the collimator alcove is added to minimize the neutron and  $\gamma$  background in the experimental hall and to satisfy the JLab RadCon radiation dose rate limit in the experimental hall (1 mrem/h), which is roughly based on the requirement to limit the yearly dose accumulation at the CEBAF boundary at 10 mrem. The key area for the dose rate evaluation is in an area of  $(6 \times 6)$  m<sup>2</sup> on ceiling of the experimental hall centered above the GlueX detector, as shown in Fig. 5. The dose rate limit at that location roughly corresponds to the expected dose rate at the CEBAF fence at the level of 1  $\mu$ rem/h, as both evaluated and observed at other locations at CEBAF (in the vicinity of the high power End Stations of Halls A and C). The Fig. 7 illustrates typical radiation dose rates currently observed around the Collimator Cave at Hall D during photon beam operation, which are generally  $\lesssim 100$  mrad/h. The task for the shielding design of the Be target assembly in the Collimator Cave for the new experiment is to keep the radiation environment in the hall at or below the typical current level, both during and after beam delivery.

A vacuum beam pipe extends between the KPT and the cryogenic target, and prevents the beam kaons and background neutrons and photons re-scattering in the air in the experimental hall. Directly downstream of the Be target there will be a sweeping magnet with a field integral of 0.8 T  $\cdot$  m to remove up the charged particle component from the beam.

## C. The Kaon and Neutron Flux

Charged particles produced by the interaction of the photon beam with the KPT are removed by a sweep magnet downstream of the KPT. The resulting beam consists primarily of neutrons and  $K_L$ 's, and in this section we calculate their properties. Neutral kaon production by bremsstrahlung photons was simulated using the PYTHIA MC generator [18]. The photon flux on the KPT face shown in Fig. 3 was used as input for Monte Carlo simulations. The main mechanism of  $K_L$  production in our energy range is via  $\phi$ -meson photoproduction, which yields the same number of  $K^0$  and  $\bar{K}^0$ .

The neutron flux calculations were performed using the MCNP radiation transport code [12], and a simplified model of the KLF beamline. The MCNP model simulated a 12 GeV 5  $\mu$ A electron beam hitting the copper radiator inside of the CPS. Electrons were transported through the copper radiator where they produced bremsstrahlung photons, which, in turn, were transported through the vacuum pipe until they hit the beryllium target. Secondary particles including neutrons and photons were traced in all components of the MCNP model. However, areas outside the concrete walls of the collimator alcove and the bremsstrahlung photon beam pipe

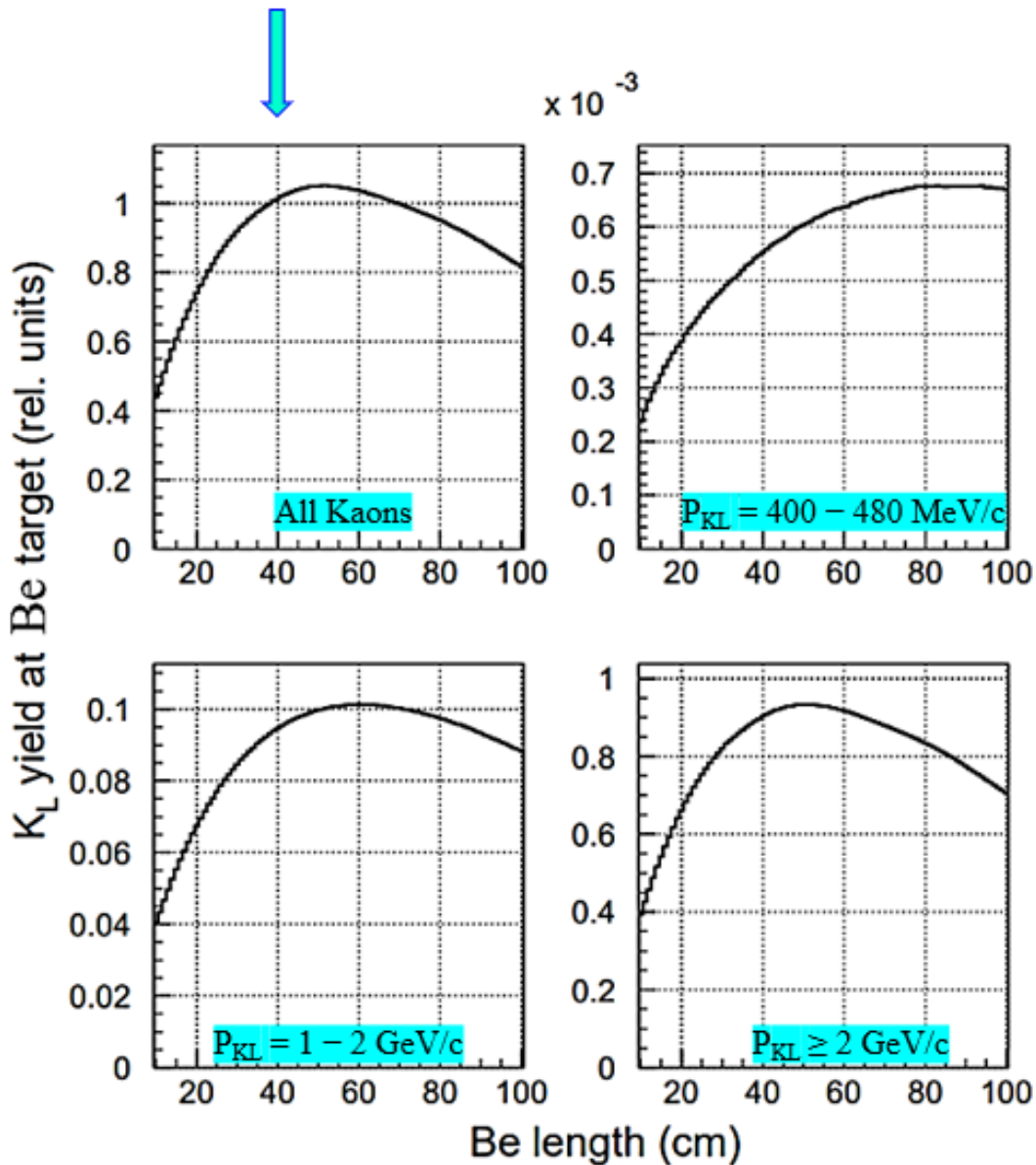


FIG. 6. Dependence of the K-long yield at the GlueX cryogenic LH<sub>2</sub> target on the thickness of the target for the different  $K_L$  momenta ranges. Top Left: For all  $K_L$  momenta,  $P_{KL}$ . Top Right: For  $P_{KL} = 400 - 480$  MeV/c. Bottom Left: For  $P_{KL} = 1 - 2$  GeV/c. Bottom Right: For  $P_{KL} \geq 2$  GeV/c.

326 were excluded from the model to increase the calculation<sup>337</sup>  
 327 speed. Additionally, we replaced the detailed models of<sup>338</sup>  
 328 the pair spectrometer and flux monitor magnets with five<sup>339</sup>  
 329 iron blocks placed around the beam pipe at the entrance  
 330 of the main experimental hall that contains GlueX spec-  
 331 trometer.

332 Fig. 8 shows that our simulations for the KLF  $K_L$  and<sup>341</sup>  
 333 neutron flux (Fig. 8 (left)), which are qualitatively similar  
 334 with the  $K_L$  spectrum measured by SLAC at 16 GeV [21]<sup>342</sup>  
 335 (Fig. 8 (right)). The KLF  $K_L$  flux is primarily over the<sup>343</sup>  
 336 range  $p(K_L) = 1 - 10$  GeV/c, with a maximum flux near<sup>344</sup>

4 GeV/c. The neutron flux falls sharply as the neutron  
 momentum increases, and is mostly limited to  $p(n) <$   
 2 GeV/c.

#### D. Neutron Flux on the Upstream Face of the GlueX Spectrometer

The neutron flux produced by the KPT has the potential to affect components of the GlueX spectrometer. The most sensitive components are the silicon photomul-

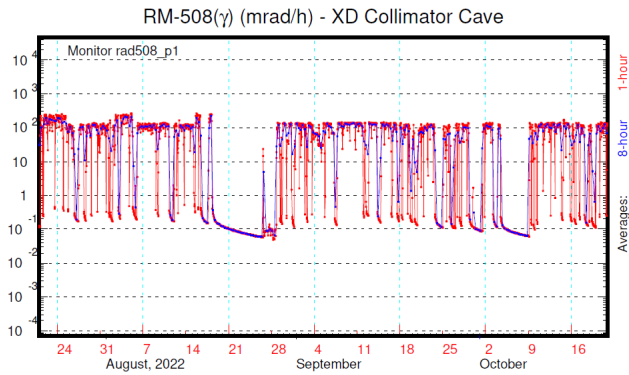


FIG. 7. A typical radiation environment in the Hall D Collimator Cave. Average hourly (red) and 8 h (blue) readings of the radiation monitors RM-508 are shown as a function of the calendar time during the Hall D operations in July-October of 2022.

tipliers (SiPMs) used for the Start Counter (SC) [23–25] and Barrel Electromagnetic Calorimeter (BCAL) [25, 26], which are located on the upstream end of the GlueX spectrometer. The SiPM detectors are only sensitive to neutron energies above 1 MeV [22]. To investigate the potential effect on these sensors, we calculated the prompt neutron dose rate for these neutron energies as a function of radial distance on the upstream end and show these results in Fig. 9 (left). The SiPMs used in the SC and BCAL are expected to tolerate this calculated neutron background. Previous studies state that the dose rate of 30 mrem/h increases the dark current at SiPM by a factor of 5 after 75 days of photon beam running [22]. The expected dose is well below this rate.

#### IV. RADIATION SAFETY REQUIREMENTS

In this section, we summarize the radiation safety requirements for the KPT and the calculations performed which show that these requirements are satisfied by the current KPT design. The task for the shielding design of the CPS in the Tagger enclosure and of the Beryllium target assembly in the Collimator Cave for the new experiment is to keep the radiation environment in their vicinity at or below the typical current level, both during and after the beam delivery. The radiation safety considerations are taken into account in the Beryllium target assembly design as explained in the Sections III.C and III.D above. The final design will be reviewed by the Radiation Physics Group at JLab for the final adjustments and approval when it is ready.

#### V. PROMPT DOSE

The prompt radiation dose in the KPT alcove affects the lifetime of materials and equipment. We calculate

the prompt dose in the region of the KPT and the adjoining labyrinth using a FLUKA simulation. The layout of this region and corresponding map of prompt dose at the nominal beam current of  $5 \mu\text{A}$  is shown in Fig. 10. These simulations show that most of the prompt radiation is contained in the KPT, and the rates outside the KPT meet the requirements of radiation safety at JLab which is 1 mrem/h [19].

As an additional check, we calculate the prompt radiation dose rate for neutrons (photons) in the experimental hall at the key area for RadCon on the ceiling using MCNP. We find a rate of  $0.27 \pm 0.08$  mrem/h ( $0.065 \pm 0.002$  mrem/h), which is also under the limit of 1 mrem/h [19].

#### VI. ACTIVATION DOSE

The FLUKA model used for the activation calculations is more complicated. It includes the CPS, tagger hall, the beam line from the tagger hall to the KPT, and the KPT along with a more extensive model of the labyrinth and the rest of the collimator cave enclosure. The activation dose equivalent rates were calculated in units of pSv/s using the FLUKA code after 1000 hours of continuous operation at the electron beam current  $5 \mu\text{A}$ . The corresponding equivalent dose rates after the end of beam delivery for 1 hour, 1 day, 1 week, and 1 month respectively are shown on Fig. 11 and summarized in Table I. According to this figure the activation level around the KPT after one hour is below the limit for high radiation area (100 mrem/h) and therefore meets the requirements of radiation safety at JLab.

The activation dose rate after 1000 h of operation in the KPT labyrinth is shown on Fig. 12. From this figure, we conclude that the dose rate near the exit from the KPT labyrinth to the main part of the experimental hall is below the JLab allowed limit of 1 mrem/h.

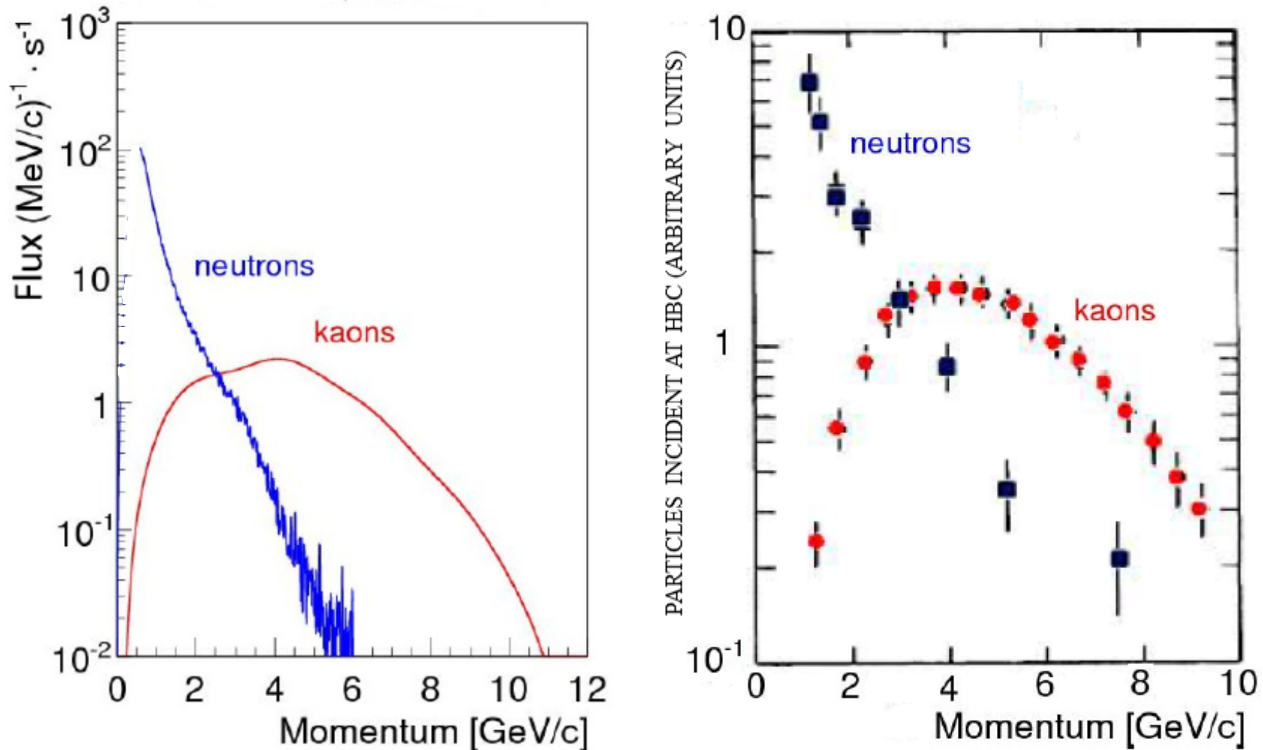


FIG. 8. fff05 The  $K_L$  and the neutron momentum spectra on the cryogenic target. Left: Rate of  $K_L$  (red) and neutrons (blue) on the LH<sub>2</sub>/LD<sub>2</sub> cryogenic target of Hall D as a function of their generated momenta, with a total rate of  $\sim 10^4$   $K_L$ /sec and  $6.6 \times 10^5$  n/sec, respectively. The  $K_L$  flux calculations were performed using Pythia generator [18] while the neutron flux calculations were performed using the MCNP transport code [12]. Right: Experimental data from SLAC measurements using a 16 GeV/c electron beam were taken from Ref. [21] (Figure 3).

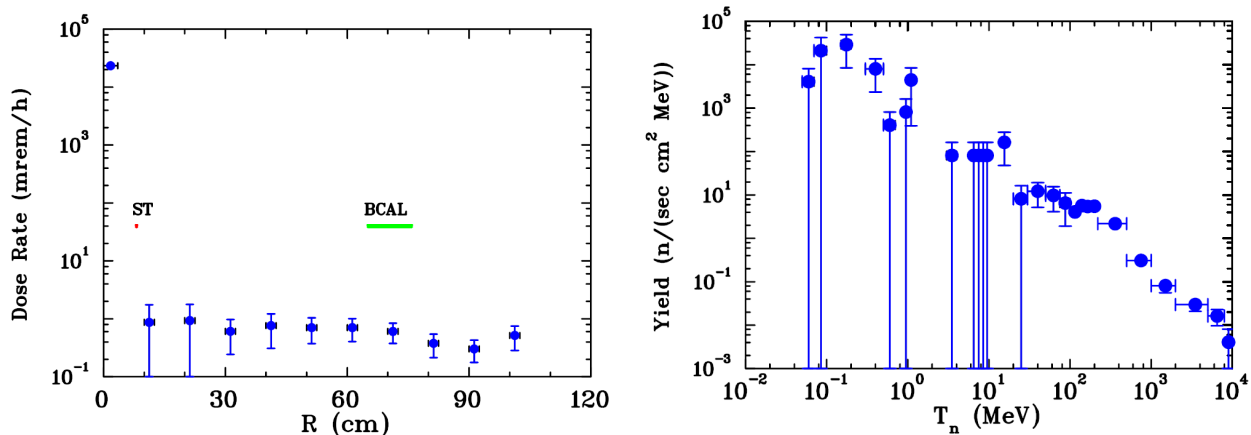


FIG. 9. fff08 Left: Prompt neutron radiation dose rate background calculated for SiPM of SC and BCAL on the face of the cryogenic target. In this case, we did not take into account additional shielding in the experimental hall. Right: Neutron energy spectrum in the beam on the face of the cryogenic target.

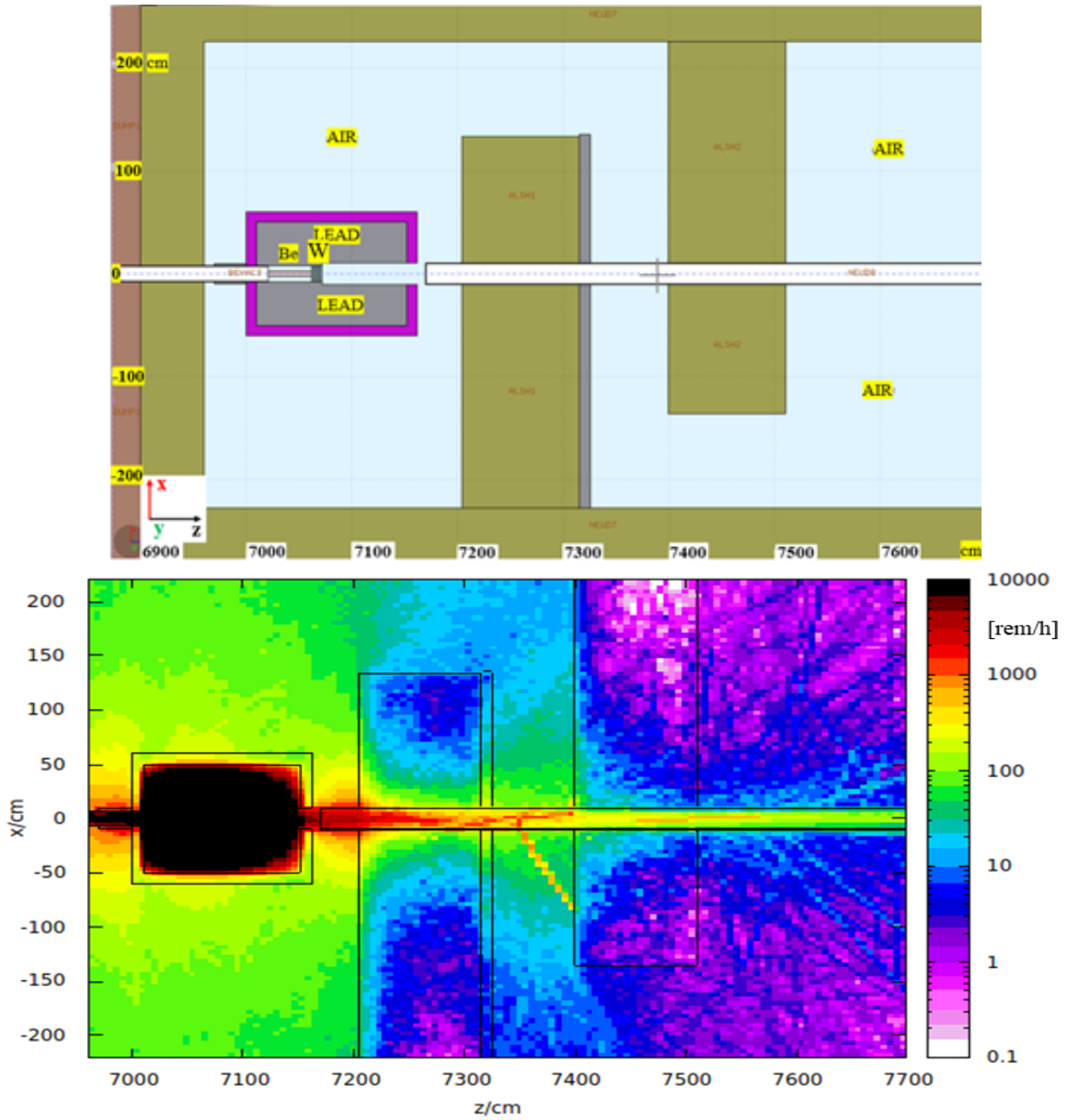


FIG. 10. fff17 Prompt dose equivalent in Collimator alcove. Top: – part of full CPS-KPT FLUKA model with KPT alcove. *brown* – soil, *khaki* – concrete, *blue* – air, *grey* – lead, *pink* – borated polyethylene. *green* – tungsten, *light pink* – beryllium. Bottom: – prompt dose equivalent map in rem/h at the electron beam current  $5 \mu\text{A}$ . Horizontal scale – coordinate along the photon beam line in cm. Vertical scale – horizontal coordinate in cm. Color scale – prompt dose equivalent in rem/h within vertical coordinate  $-150 < y/\text{cm} < 150$  relative to the beam line. From these plots, we conclude that the equivalent dose level around the KPT meets the requirements of the radiation safety at JLab.

TABLE I. Activation estimates around KPT assembly at  $r = 90 \text{ cm}$ ,  $7000 \text{ cm} < z < 7150 \text{ cm}$ .

Activation after one (units)	Hour	Day	Week	Month
pSv/s	$3.5 \times 10^4$	$2 \times 10^4$	$0.5 \times 10^3$	$1 \times 10^2$
mrem/h	13	8	0.2	0.04



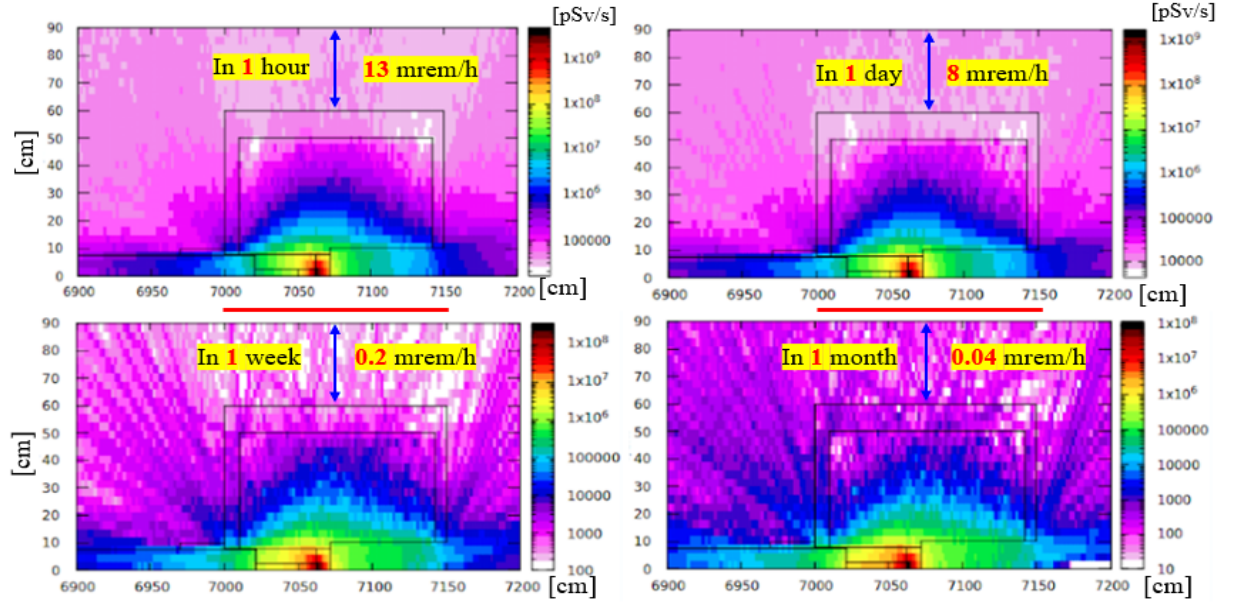


FIG. 11. fff177 Activation dose in materials of KPT and around it's surface after 1000 hours of continuous operation at electron beam current  $5 \mu\text{A}$  and energy  $12 \text{ GeV}$ . Equivalent dose in pSv/s after 1 hour accelerator operational pause. Top Left: - After one hour. Top Right: - After one day. Bottom Left: - After one week. Bottom Right: - After one month. Horizontal scale - coordinate along the photon beam line in cm. Vertical scale - radial coordinate in cm. Color scale - equivalent dose in pSv/s. Equivalent dose  $10^5 \text{ pSv/s} = 36 \text{ mrem/h}$ . The numerical estimates of activated dose at 30 cm distance from the KPT surface ( $r/cm = 90, 7000 < z/cm < 7150$ ) are given in Table I. From these plots, we conclude that the activation level around the KPT meets the requirements of the radiation safety at JLab.

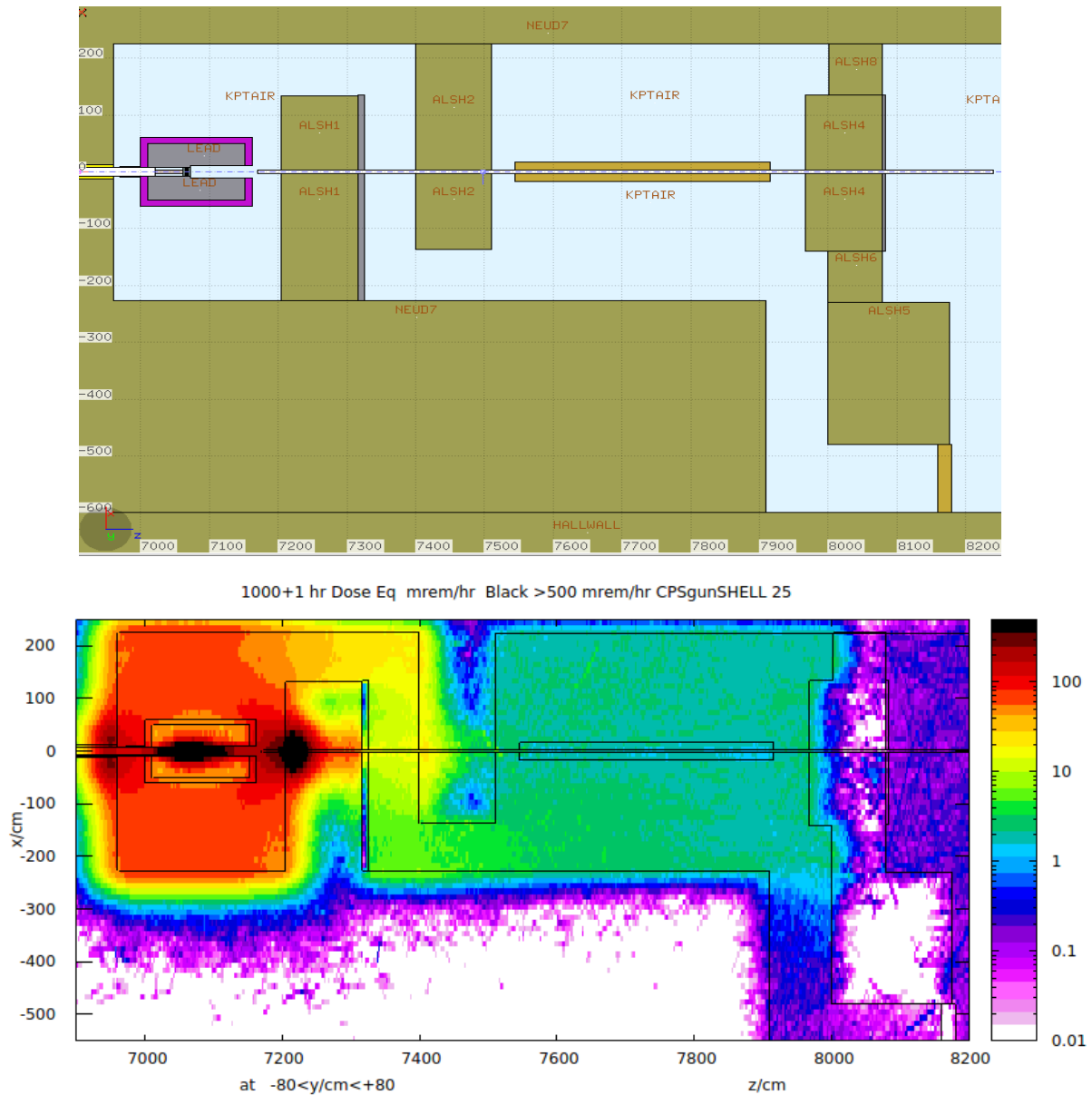


FIG. 12. fff1776 Activation dose in KPT labyrinth after 1000 hours of continuous operation at electron beam current  $5 \mu\text{A}$  and energy 12 GeV. Top: Plan view of the KPT labyrinth. Entry door is marked with red color. Vertical scale - in hall horizontal coordinate  $x$  in cm. Horizontal scale - in hall coordinate along beam  $z$  in cm. Bottom: Equivalent dose in mrem/hr after 1 hour accelerator operational pause. Horizontal scale - coordinate along the photon beam line in cm. Vertical scale - horizontal coordinate in cm. Color scale - equivalent dose in mrem/hr. Equivalent dose  $10^5 \text{ pSv/s} = 36 \text{ mrem/h}$ . From these plots, we conclude that the activation level near the exit from KPT labyrinth meets the requirements of the radiation safety at JLab ( below 1 mrem/hr).

## VII. SIMULATION OF POWER DEPOSITION IN KPT

In this Section, we consider the power distribution in the KPT. We have calculated this distribution using a simplified model of the corresponding beamline using the FLUKA software [30].

### A. Beam Line Model in FLUKA

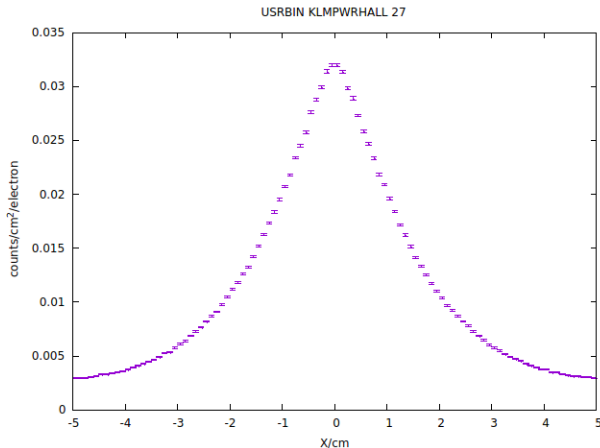


FIG. 13. Secondary photon beam profile at the entry of the Be target. Vertical scale - emission probability in a.u, horizontal scale - photon coordinate across the target in cm.

The simplified beamline model was developed with a goal to provide high rate of calculations. The 12 GeV electron beam hits the copper target 1.4 mm thick (10% of its radiation length). The photon beam propagates to a 67 m distance where it hits the beryllium target. The secondary photon beam is very well focused on the Be target 6 cm in diameter – the photon beam profile on the Beryllium target is shown in Fig. 13

### B. Energy Deposition in the Kaon Production Target

The FLUKA model of the kaon production target assembly is shown in Fig. 14.

The energy deposition map inside the target is shown in Fig. 15. The color scale is given for the energy deposition in units of  $\text{GeV}/\text{cm}^3/\text{electron}$ . In order to estimate the power density in  $\text{GeV}/\text{cm}^3/\text{s}$  this value has to be scaled by the electron beam intensity of  $3 \times 10^{13}$  electrons/s at the nominal beam current  $5 \mu\text{A}$ . In order to convert it to  $\text{Watts}/\text{cm}^3$  an additional scale factor of  $1.6 \times 10^{-10}$  J/GeV is required. For example, the maximum energy deposition  $0.01 \text{ GeV}/\text{cm}^3/\text{electron}$  translates to  $48 \text{ W}/\text{cm}^3$ .

The effect of the tails of the photon beam that pass through the beam pipe is clearly seen in Fig. 15 at the entry to the KPT. This can also be seen by comparing the projection along the z-coordinate for the full KPT (Fig. 16), and for  $R < 4$  cm, which consists mostly of the Be target and tungsten plug (Fig. 17). So, the photon beam tails create an additional source of radiation from the surface of the KPT.

We note that the spectrum of photons on the face of the Be-target generated using this simplified model by FLUKA agrees well (within  $\approx 10\%$ ) with the detailed MCNP calculations for  $E_\gamma > 0.2$  MeV and simple analytical models.

## VIII. HEATING

The tungsten absorber block with dimensions of  $(15.25 \times 15.25 \times 10) \text{ cm}^3$  will absorb most of the photon beam energy totaling over 5 KW in power. Therefore, it is necessary to cool the absorber with water to prevent any of the lead parts of the KPT assembly from melting. Figure 18 shows the water cooling setup for the tungsten plug which consists of four copper plates cooled with water at  $35^\circ\text{C}$  supply temperature. The copper tubes are soldered to the copper plate. The cooling system is designed to provide 2 gallons/min water flow through the tubes.

We performed a detailed study with steady-state thermal analysis using simulated data from the FLUKA model for the power absorption in the tungsten block described in the previous Section VII as the input for the calculations. The temperature calculations include the heat transfer through the homogeneous tungsten material towards the copper plates on the sides as well as the heat transfer from the copper to the cooling water flowing through the tubes.

Figure 19 shows the temperature distributions in the absorber versus x- and y-coordinates (left) at the depth of  $z = 2.5$  cm inside the tungsten block, and the temperature versus r- and z-coordinates at the azimuthal angle of  $\phi = 45^\circ$  (right). The cooling copper plates surrounding the tungsten plug are not shown in this Figure. Figure 20 shows the temperature dependence on the radial coordinate at the  $z = 2.5$  cm depth and at azimuthal angle  $\phi = 45^\circ$  (left), and the dependence on the z-coordinates at  $r = 0$  cm and the azimuthal angle of  $\phi = 45^\circ$  (right). The results show that the maximum temperature inside the tungsten plug will be at the depth of about  $z = 2.5$  cm inside the tungsten block along the beam, and the value of the temperature at that point is expected to be  $220^\circ\text{C}$  with the described cooling configuration. The temperature at the sides of the tungsten plug at the depth of the maximum heat deposition  $z = 2.5$  cm and in the horizontal plane on the beamline level is expected to be around  $65^\circ\text{C}$ . The temperature at the upstream face of the tungsten plug at the point of beam impact is expected to be around  $180^\circ\text{C}$ . Based on these results, we conclude that

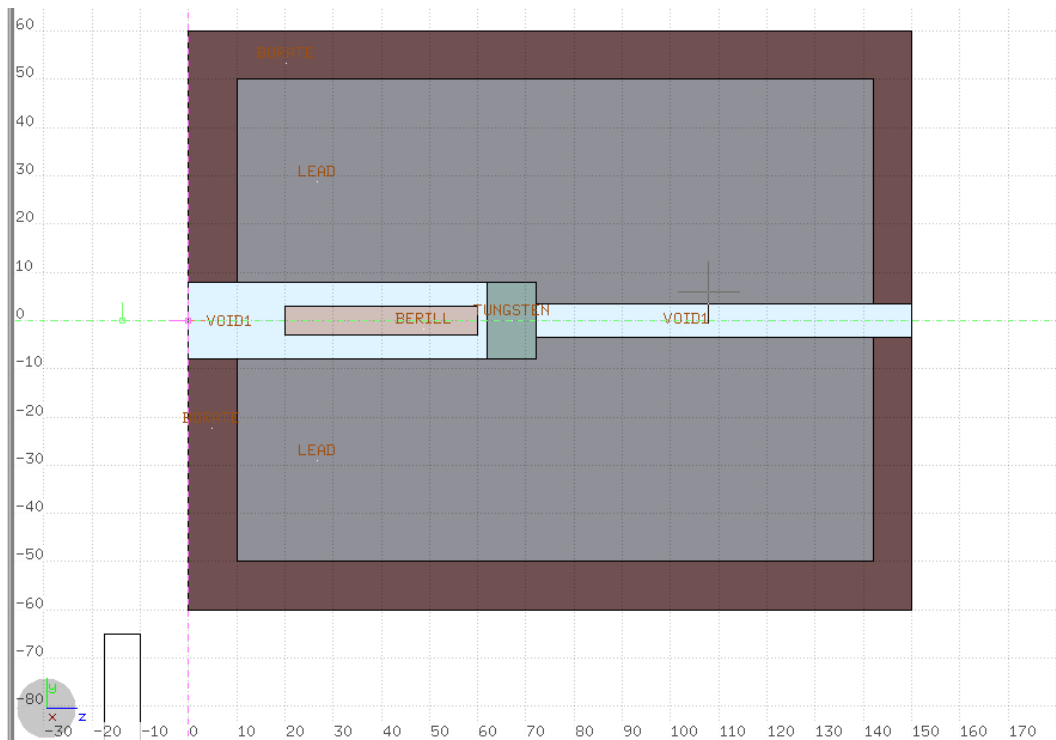


FIG. 14. The FLUKA model of the Kaon Production Target assembly. Vertical scale -  $R$ -coordinates, horizontal scale - coordinate along photon beam directions. Be “target” is a cylinder (light pink), 6 cm diameter and 40 cm long in a air filled pipe 8 cm in radius. The Be target length corresponds to 1.75 r.l. and was optimized at SLAC. It was shown that the further increase of the length of the target is not effective as it leads to the rapid falloff of  $K_L$  momentum spectrum [21]. Following the target is a “plug” of tungsten (light green) 8 cm radius and 10 cm thick, which is followed by an open pipe 5 cm radius; the Pb-shield is a cylinder (light blue) with sizes  $R \times L = (50 \times 132)$  cm<sup>2</sup>; the  $B$ -doped polyethylene layer (brawn) is sized as  $(60 \times 150)$  cm<sup>2</sup>. A “black wall” located at  $z = -20$  cm with a hole of 3 cm by radius may be placed in front of the target to form a beam profile shown in Fig. 13(top).

496 the current design for the tungsten plug cooling system<sup>514</sup>  
 497 is sufficient to prevent any significant overheating of the<sup>515</sup>  
 498 material around the tungsten. <sup>516</sup>

there will be some actual contact. 300 W is applied to a  
 theoretical 1 mm diameter hole over the entire length of  
 the cylindrical surface.

#### 499 A. Beryllium Target Cooling <sup>517</sup>

500 Since there is a concern with air contamination from<sup>518</sup>  
 501 the beryllium if air is blown onto the surface for cooling,<sup>519</sup>  
 502 it is decided to use water cooling for this target (Fig. 21).<sup>520</sup>  
 503 A maximum temperature of 66°C was found in the beryl-<sup>521</sup>  
 504 lium. The target is wrapped with a 0.065 inch thick cop-<sup>522</sup>  
 505 per sheet in which 0.25 inch cooling tubes are brazed on<sup>523</sup>  
 506 to. The inner surface of the water cooling tube is assumed<sup>524</sup>  
 507 to have a convection coefficient of 5,000 W/m<sup>2</sup> K and a<sup>525</sup>  
 508 water temperature of 40°C on average. Hand calcula-<sup>526</sup>  
 509 tions and ANSYS steady state thermal calculations [32]<sup>527</sup>  
 510 are in close agreement. The model takes into consid-<sup>528</sup>  
 511 eration imperfect thermal contact between the beryllium<sup>529</sup>  
 512 and copper cooling sheet by incorporating a 100 μ air gap<sup>530</sup>  
 513 between the 2 surfaces. This is very conservative since<sup>531</sup>

## IX. SUMMARY

In this document, we have described a conceptual de-  
 sign for a Kaon Production Target that satisfies the re-  
 quirements of the KLF project as well as the physical  
 and radiological requirements of Jefferson Lab.

Simulations were performed to optimize the dimen-  
 sions of the target and various shielding configurations  
 with a goal to maximize the flux of  $K_L$ 's keeping neutron  
 and gamma radiation at the level limited by the safety  
 requirements at Jefferson Lab. The resulting kaon flux is  
 $\sim 10^4$   $K_L$ /sec, which meets the requirements for the KLF  
 project, while the neutron and gamma fluxes and corre-  
 sponding prompt dose rates are safely below the radiation  
 dose rate limits established by the Radiology Control Di-  
 vision of Jefferson Lab.

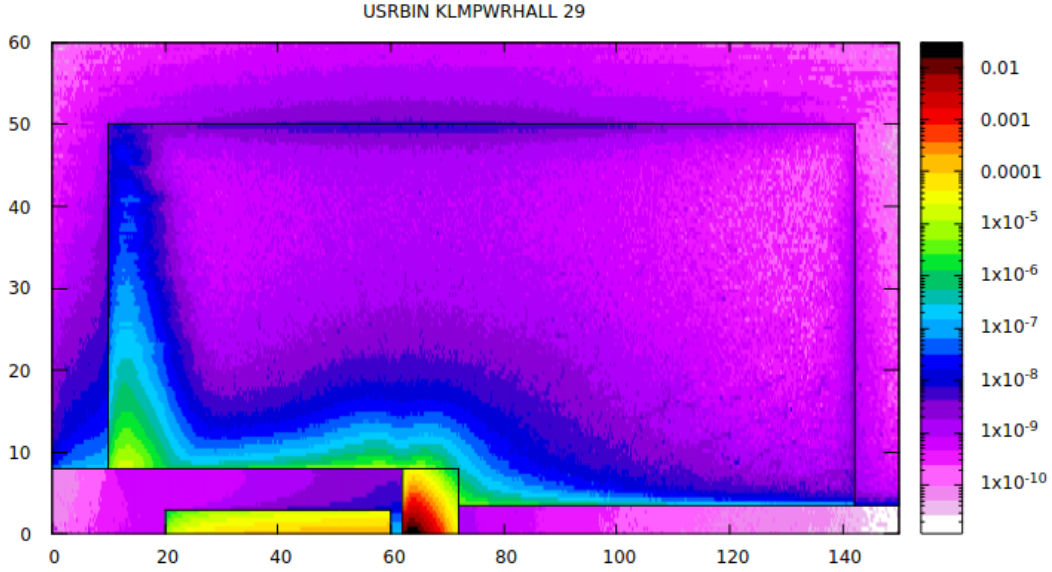


FIG. 15. Energy deposition inside the borated shielding cylinder of the KLF KPT. Vertical scale – radial coordinate in cm, horizontal scale –  $Z$ -coordinate along the photon beam in cm. Color scale – energy deposition in  $\text{GeV}/\text{cm}^3/\text{e}$ .

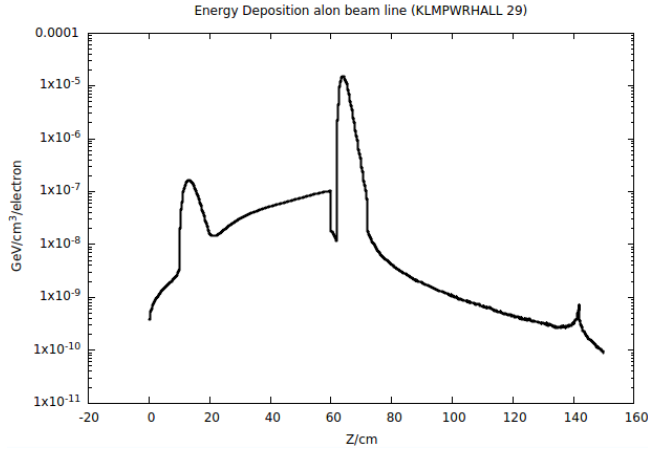


FIG. 16. Power distribution in KPT target along its  $z$ -coordinate.

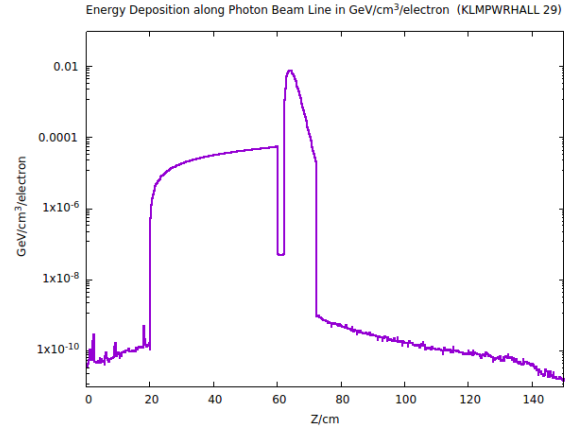


FIG. 17. Power distribution along  $Z$ -axis for  $R < 4$  cm, *i.e.*, in the cylinders of the Be target and tungsten plug.

532 Since significant beam power is deposited in the central  
 533 part of the KPT, special attention was devoted study-  
 534 ing the heat distribution inside KPT. The temperature  
 535 map inside KPT was obtained using the ANSYS soft-  
 536 ware package using the energy deposition map from the  
 537 FLUKA as an input, and no overheating elements were  
 538 found.

## 539 X. ACKNOWLEDGMENTS

540 We are thankful to Stephanie Worthington for details  
 541 of the geometry of the collimator alcove. This work was

542 supported in part by the U. S. Department of Energy, Of-  
 543 fice of Science, Office of Nuclear Physics under Awards  
 544 Nos. DE-SC0016583, DE-FG02-96ER40960, DE-  
 545 AC05-06OR23177, and DE-FG02-92ER40735, and also  
 by the U. K. STFC ST/L00478X/1 and ST/P004008/1  
 grants.



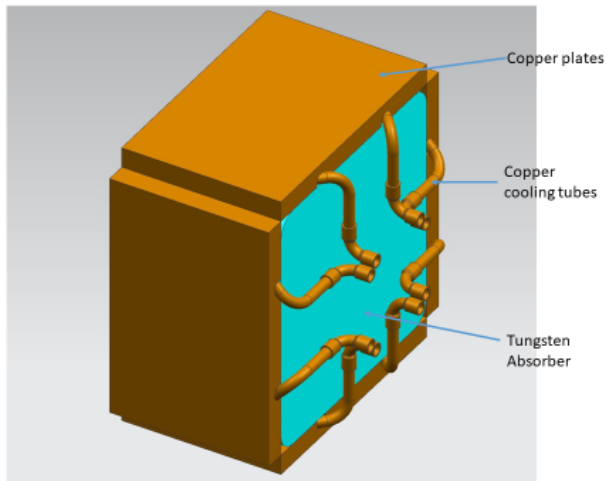


FIG. 18. Tungsten absorber cooling setup. The teal color rectangular block represents the tungsten absorbed while the copper cooling system is represented with golden brown color.

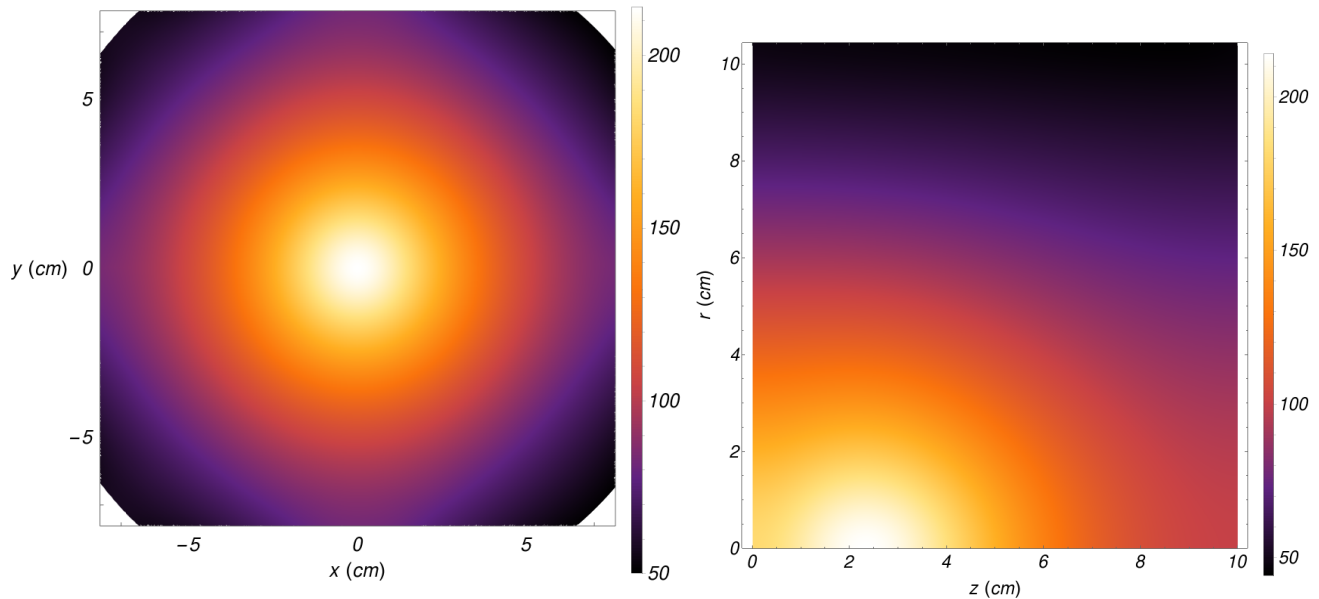


FIG. 19. fff1244 Temperature distribution inside the tungsten absorber versus x- and y-coordinates at the depth of  $z = 2.5$  cm along the beam direction inside the tungsten block (left), and temperature versus radial and axial coordinates at an azimuthal angle of  $\phi = 45^\circ$  (right).

548 [1] *Strange hadron spectroscopy with secondary  $K_L$  beam in*  
 549 *Hall D*, Spokespersons: M. J. Amarian, M. Bashkanov,  
 550 S. Dobbs, J. Ritman, J. R. Stevens, and I. I. Strakovsky  
 551 (KLF Collaboration), JLab C2-12-19-001, Newport  
 552 News, VA, USA, 2019; [arXiv:2008.08215 [nucl-ex]].  
 553 [2] S. Adhikari *et al.* [GlueX Collaboration], “The GLUEX  
 554 beamline and detector,” Nucl. Instrum. Meth. A **987**,  
 555 164807 (2021).

[3] A. Aprahamian *et al.*, *Reaching for the horizon:  
 The 2015 long range plan for nuclear science*;  
<http://science.energy.gov/np/nsac/> .  
 [4] PAC48 Final Report,  
[https://www.jlab.org/exp\\_prog/PACpage/PAC48/PAC48\\_](https://www.jlab.org/exp_prog/PACpage/PAC48/PAC48_PrelimReportPlus_FINAL.pdf)  
 PrelimReportPlus\_FINAL.pdf .  
 [5] D. Day *et al.*, “A conceptual design study of a Compact  
 Photon Source (CPS) for Jefferson Lab,” Nucl. Instrum.

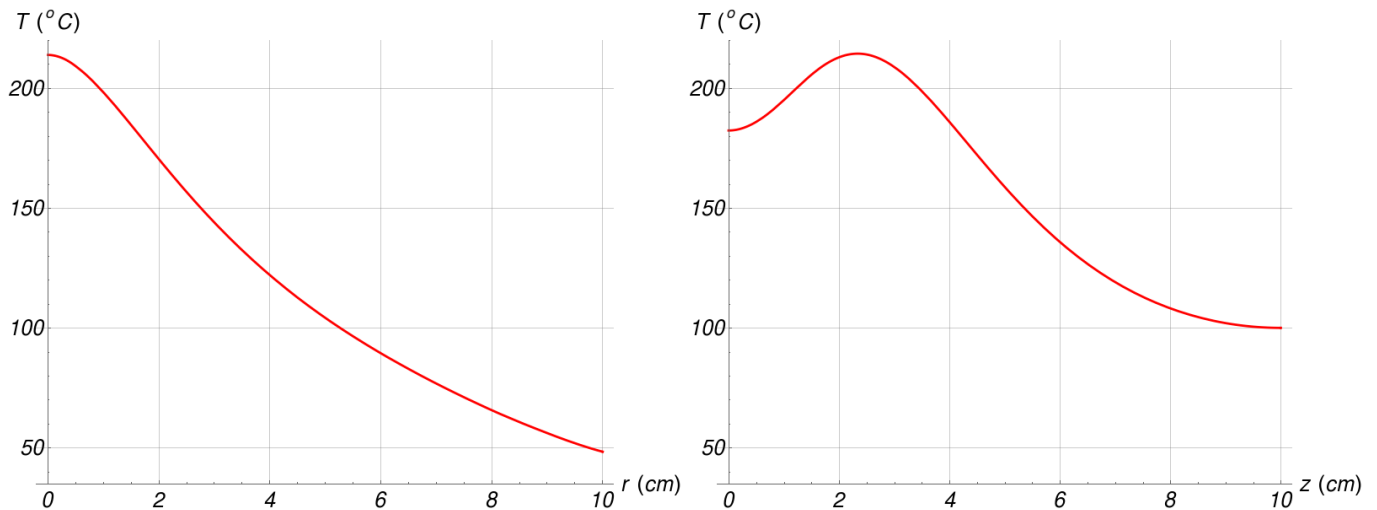


FIG. 20. fff1245 Temperature inside the tungsten absorber versus radial coordinate  $r$  at the  $z = 2.5$  cm depth and  $\phi = 45^\circ$  azimuthal angle (left), and temperature versus  $z$  along the beamline at  $r = 0$  cm and the azimuthal angle of  $\phi = 45^\circ$  (right).

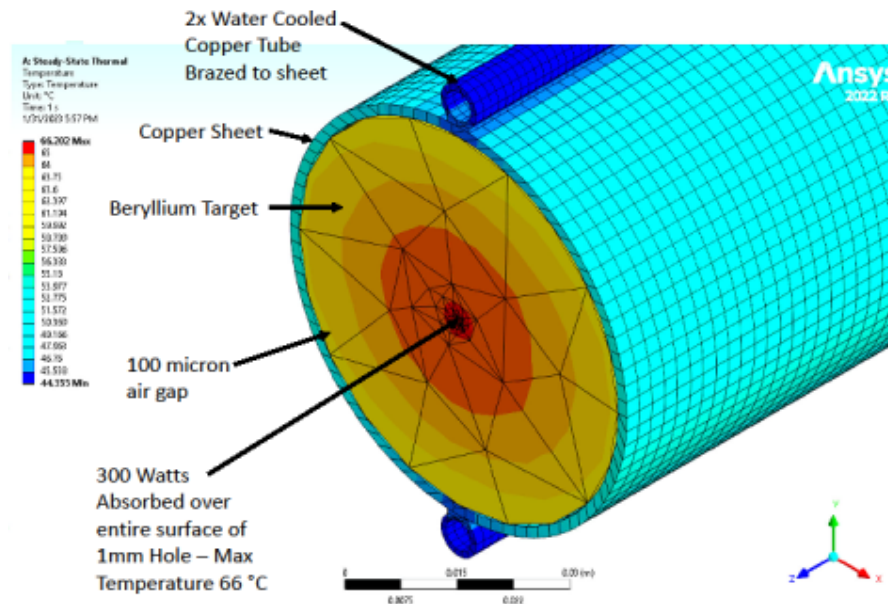


FIG. 21. Water cooled Beryllium target ANSYS results.

- 564 Methods, A **957**, 163429 (2020). 577
- 565 [6] V. Baturin, M. Amarian, E. Chudakov, P. Degtyarenko, S. Dobbs, H. Egiyan, C. E. Hyde, I. Strakovsky, and S. T. Whitlatch, “The Compact Photon Source for Hall D at Jefferson Laboratory (Technical Note),” in progress. 580
- 566 581
- 567 [7] M. Bashkanov, D. P. Watts, N. Zachariou, E. Chudakov, M. Amarian, J. Ritman, J. Stevens, and I. Strakovsky, “KL flux monitor,” Preprint GlueX-doc-3603, 2019. 584
- 568 585
- 569 [8] R. Yamartino *et al.*, “A study of the reactions  $\bar{K}^0 p \rightarrow \Lambda \pi^+$  and  $\bar{K}^0 p \rightarrow \Sigma^0 \pi^+$  from 1-GeV/c to 12-GeV/c,” Phys. Rev. D **10**, 9 (1974); R. Yamartino, “A study of the reactions  $\bar{K}^0 p \rightarrow \Lambda \pi^+$  and  $\bar{K}^0 p \rightarrow \Sigma^0 \pi^+$  from 1-GeV/c to 12-GeV/c,” SLAC-R-0177, SLAC-R-177, SLAC-0177, 589
- 570 582
- 571 583
- 572 584
- 573 585
- 574 586
- 575 587
- 576 588
- 589 590
- 591 592
- 593 594
- 595 595
- 596 596
- 597 597
- 598 598
- 599 599
- 600 600
- 601 601
- 602 602
- 603 603
- 604 604
- 605 605
- 606 606
- 607 607
- 608 608
- 609 609
- 610 610
- 611 611
- 612 612
- 613 613
- 614 614
- 615 615
- 616 616
- 617 617
- 618 618
- 619 619
- 620 620
- 621 621
- 622 622
- 623 623
- 624 624
- 625 625
- 626 626
- 627 627
- 628 628
- 629 629
- 630 630
- 631 631
- 632 632
- 633 633
- 634 634
- 635 635
- 636 636
- 637 637
- 638 638
- 639 639
- 640 640
- 641 641
- 642 642
- 643 643
- 644 644
- 645 645
- 646 646
- 647 647
- 648 648
- 649 649
- 650 650
- 651 651
- 652 652
- 653 653
- 654 654
- 655 655
- 656 656
- 657 657
- 658 658
- 659 659
- 660 660
- 661 661
- 662 662
- 663 663
- 664 664
- 665 665
- 666 666
- 667 667
- 668 668
- 669 669
- 670 670
- 671 671
- 672 672
- 673 673
- 674 674
- 675 675
- 676 676
- 677 677
- 678 678
- 679 679
- 680 680
- 681 681
- 682 682
- 683 683
- 684 684
- 685 685
- 686 686
- 687 687
- 688 688
- 689 689
- 690 690
- 691 691
- 692 692
- 693 693
- 694 694
- 695 695
- 696 696
- 697 697
- 698 698
- 699 699
- 700 700
- 701 701
- 702 702
- 703 703
- 704 704
- 705 705
- 706 706
- 707 707
- 708 708
- 709 709
- 710 710
- 711 711
- 712 712
- 713 713
- 714 714
- 715 715
- 716 716
- 717 717
- 718 718
- 719 719
- 720 720
- 721 721
- 722 722
- 723 723
- 724 724
- 725 725
- 726 726
- 727 727
- 728 728
- 729 729
- 730 730
- 731 731
- 732 732
- 733 733
- 734 734
- 735 735
- 736 736
- 737 737
- 738 738
- 739 739
- 740 740
- 741 741
- 742 742
- 743 743
- 744 744
- 745 745
- 746 746
- 747 747
- 748 748
- 749 749
- 750 750
- 751 751
- 752 752
- 753 753
- 754 754
- 755 755
- 756 756
- 757 757
- 758 758
- 759 759
- 760 760
- 761 761
- 762 762
- 763 763
- 764 764
- 765 765
- 766 766
- 767 767
- 768 768
- 769 769
- 770 770
- 771 771
- 772 772
- 773 773
- 774 774
- 775 775
- 776 776
- 777 777
- 778 778
- 779 779
- 780 780
- 781 781
- 782 782
- 783 783
- 784 784
- 785 785
- 786 786
- 787 787
- 788 788
- 789 789
- 790 790
- 791 791
- 792 792
- 793 793
- 794 794
- 795 795
- 796 796
- 797 797
- 798 798
- 799 799
- 800 800
- 801 801
- 802 802
- 803 803
- 804 804
- 805 805
- 806 806
- 807 807
- 808 808
- 809 809
- 810 810
- 811 811
- 812 812
- 813 813
- 814 814
- 815 815
- 816 816
- 817 817
- 818 818
- 819 819
- 820 820
- 821 821
- 822 822
- 823 823
- 824 824
- 825 825
- 826 826
- 827 827
- 828 828
- 829 829
- 830 830
- 831 831
- 832 832
- 833 833
- 834 834
- 835 835
- 836 836
- 837 837
- 838 838
- 839 839
- 840 840
- 841 841
- 842 842
- 843 843
- 844 844
- 845 845
- 846 846
- 847 847
- 848 848
- 849 849
- 850 850
- 851 851
- 852 852
- 853 853
- 854 854
- 855 855
- 856 856
- 857 857
- 858 858
- 859 859
- 860 860
- 861 861
- 862 862
- 863 863
- 864 864
- 865 865
- 866 866
- 867 867
- 868 868
- 869 869
- 870 870
- 871 871
- 872 872
- 873 873
- 874 874
- 875 875
- 876 876
- 877 877
- 878 878
- 879 879
- 880 880
- 881 881
- 882 882
- 883 883
- 884 884
- 885 885
- 886 886
- 887 887
- 888 888
- 889 889
- 890 890
- 891 891
- 892 892
- 893 893
- 894 894
- 895 895
- 896 896
- 897 897
- 898 898
- 899 899
- 900 900
- 901 901
- 902 902
- 903 903
- 904 904
- 905 905
- 906 906
- 907 907
- 908 908
- 909 909
- 910 910
- 911 911
- 912 912
- 913 913
- 914 914
- 915 915
- 916 916
- 917 917
- 918 918
- 919 919
- 920 920
- 921 921
- 922 922
- 923 923
- 924 924
- 925 925
- 926 926
- 927 927
- 928 928
- 929 929
- 930 930
- 931 931
- 932 932
- 933 933
- 934 934
- 935 935
- 936 936
- 937 937
- 938 938
- 939 939
- 940 940
- 941 941
- 942 942
- 943 943
- 944 944
- 945 945
- 946 946
- 947 947
- 948 948
- 949 949
- 950 950
- 951 951
- 952 952
- 953 953
- 954 954
- 955 955
- 956 956
- 957 957
- 958 958
- 959 959
- 960 960
- 961 961
- 962 962
- 963 963
- 964 964
- 965 965
- 966 966
- 967 967
- 968 968
- 969 969
- 970 970
- 971 971
- 972 972
- 973 973
- 974 974
- 975 975
- 976 976
- 977 977
- 978 978
- 979 979
- 980 980
- 981 981
- 982 982
- 983 983
- 984 984
- 985 985
- 986 986
- 987 987
- 988 988
- 989 989
- 990 990
- 991 991
- 992 992
- 993 993
- 994 994
- 995 995
- 996 996
- 997 997
- 998 998
- 999 999
- 1000 1000

- SLAC-177.
- [9] S. Adhikari *et al.* [GlueX Collaboration], “Beam asymmetry  $\Sigma$  for the photoproduction of  $\eta$  and  $\eta'$  mesons at  $E_\gamma = 8.8$  GeV,” Phys. Rev. C **100**, 052201 (2019).
- [10] A. Ali *et al.* [GlueX Collaboration], “First measurement of near-threshold  $J/\psi$  exclusive photoproduction off the proton,” Phys. Rev. Lett. **123**, 072001 (2019).
- [11] H. Al Ghouli *et al.* [GlueX Collaboration], “Measurement of the beam asymmetry  $\Sigma$  for  $\pi^0$  and  $\eta$  photoproduction on the proton at  $E_\gamma = 9$  GeV,” Phys. Rev. C **95**, 042201 (2017)
- [12] T. Goorley *et al.*, “Initial MCNP6 release overview,” Nucl. Tech. **180**, 298. (2012); <https://mcnp.lanl.gov/>.

- [13] A. D. Brody *et al.*, “Production of  $K^0(2)$  mesons and neutrons by 10-GeV and 16-GeV electrons on beryllium,” *Phys. Rev. Lett.* **22**, 966 (1969). 625-627
- [14] M. G. Albrow *et al.*, “Photoproduction of  $K^0$  mesons from protons and from complex nuclei,” *Nucl. Phys. B* **23**, 509 (1970). 628-630
- [15] N. Petoussi-Henss, W. E. Bolch, K. F. Eckerman, A. Endo, N. Hertel, J. Hunt, M. Pelliccioni, H. Schlattl, and M. Zankl, *ICRP, 2010. Conversion Coefficients for Radiological Protection Quantities for External Radiation Exposures*, ICRP 116 Publication, Editor C. H. Clement, Ann. ICRP, **40**, (2-5) (2010). 631-636
- [16] R. G. Williams III, C. J. Gesh, and R. T. Pagh, *Compendium of material composition data for radiation transport modeling*, PNNL-15870, 2006. 637-639
- [17] G. Battistoni, T. Boehlen, F. Cerutti, P. W. Chin, L. S. Esposito, A. Fassò, A. Ferrari, A. Lechner, A. Empl, A. Mairani *et al.* “Overview of the FLUKA code,” *Annals Nucl. Energy* **82**, 10 (2015); version FLUKA2021.2.9. 640-643
- [18] We used a modified version of the Pythia [20] package for the GlueX Collaboration at JLab Hall D, <http://home.thep.lu.se/torbjorn/Pythia.html>. 644-646
- [19] Pavel Degterenko, private communication. 647
- [20] T. Sjöstrand *et al.*, “An introduction to PYTHIA 8.2,” *Comput. Phys. Commun.* **191**, 159 (2015). 648-649
- [21] G. W. Brandenburg *et al.*, “Production of  $K^0(1)$  mesons and neutrons from electrons on beryllium above 10-GeV,” *Phys. Rev. D* **7**, 708 (1973). 650-652
- [22] A. Somov, “Neutron background estimates in the Tagger hall,” Preprint GlueX-doc-1646, 2011. 653
- [23] Y. Qiang, C. Zorn, F. Barbosa, and E. Smith, “Radiation hardness tests of SiPMs for the JLab Hall D Barrel Calorimeter,” *Nucl. Instrum. Meth. A* **698**, 234 (2013). 654
- [24] E. Pooser *et al.*, “The GlueX start counter detector,” *Nucl. Instrum. Meth. A* **927**, 330 (2019). 655-658
- [25] P. Degtiarenko, A. Fass, G. Kharashvili, and A. Somov, “Calculation of radiation damage to silicon photomultipliers in GlueX experiment,” Preprint JLAB-TN-11-005, 2011.
- [26] T. D. Beattie *et al.*, “Construction and performance of the Barrel Electromagnetic Calorimeter for the GlueX experiment,” *Nucl. Instrum. Meth. A* **896**, 24 (2018).
- [27] L. Keller, private communication, 2015.
- [28] J. Allison *et al.*, “Recent developments in Geant4,” *Nucl. Instrum. Meth. A* **835**, 186 (2016).
- [29] I. Larin, “Simulation study of KL beam: KL rates and background,” in: *Workshop on Physics with Neutral Kaon Beam at JLab*, mini-Proceedings, arXiv:1604.02141 [hep-ph] (February, 2016), p. 198.
- [30] T. T. Böhlen, F. Cerutti, M. P. W. Chin, A. Fassò, A. Ferrari, P. G. Ortega, A. Mairani, P. R. Sala, G. Smirnov, and V. Vlachoudis, “The FLUKA code: Developments and challenges for high energy and medical applications,” *Nucl. Data Sheets* **120**, 211 (2014).
- [31] R. L. Workman [Particle Data Group], “Review of Particle Physics,” *PTEP* **2022**, 083C01 (2022).
- [32] ANSYS inc. Workbench 2022 R2 Finite Element Program.
- [33] I. Strakovsky, M. Amaryan, M. Bashkanov, W. J. Briscoe, E. Chudakov, P. Degtyarenko, S. Dobbs, A. Laptev, I. Larin, A. Somov *et al.* “Conceptual design of beryllium target for the KLF project,” [arXiv:2002.04442 [physics.ins-det]].

#### Appendix A: KPT Shield Layers and Weight

The approximation for the KPT weight (about 15,500 kg) and components for the Collimator cave breakdown is given in Table II.

TABLE II. Cost estimates for the KPT and its main parts by Timothy Whitlatch. One need to add about \$1K for cooling system for the beryllium. Total weight of the Be-target assembly is about 15, 500 kg.

KPT Component	Qty	Cost each (\$)	Fab cost (\$)	Total Cost (\$)
Beryllium target	1	11,000		11,000
Beryllium support	1	1,100		1,100
Tungsten absorber	1	12,000		12,000
Target lead bricks	1,190	50	2,000	61,500
Target Support structure	1	0	9,000	9,000
Hilman rollers	4	850		3,400
Rails	2		1,850	1,850
Wedge levelers	4	700		2,800
Leveler base plate	4		2,100	2,100
Borated poly sheets	24	583	4,800	18,792
Central support tubes	2	800		1,600
Hardware	76	2.5		190
Cooling plates	4	1,240		4,960
Water cooling system	1	20,000		20,000
Shielding wall lead bricks	792	50		39,600
Vacuum beamline	1	5,000		5,000
Concrete block shielding wall	1,188	5		5,940
Support for shield wall	2	3,300		6,600
Total				207,432